Repeated out-of-Africa expansions of *Helicobacter pylori* driven by replacement of deleterious mutations

Harry A. Thorpe[1&], Elise Tourrette[2&], Koji Yahara[3&], Filipa F. Vale[4], Siqi Liu[2], Mónica Oleastro[5], Teresa Alarcon[6], TsachiTsadok Perets[7], Saeid Latifi-Navid[8], Yoshio Yamaoka[9], Beatriz Martinez-Gonzalez[10], Ioannis Karayiannis[10], Timokratis Karamitros[10], Dionyssios N. Sgouras[10], Wael Elamin[11,12], Ben Pascoe[13], Samuel K. Sheppard[13], Jukka Ronkainen[14,15], Pertti Aro[16], Lars Engstrand[17], Lars Agreus[18], Sebastian Suerbaum[19, 20, 21§], Kaisa Thorell[22, 23§], Daniel Falush[2*§]

1 Institute of Basic Medical Sciences, University of Oslo, Oslo, harry.thorpe@medisin.uio.no
2 Centre for Microbes Development and Health, Institute Pasteur Shanghai. sqliu@ips.ac.cn, danielfalush@googlemail.com, elise.tourrette@gmail.com
3 Antimicrobial Resistance Research Center, National Institute of Infectious Diseases, Toyo, Japan, k-yahara@nih.go.jp
4 Pathogen Genome Bioinformatics and Computational Biology, Research Institute for Medicines (iMed-ULisboa), Faculty of Pharmacy, Universidade de Lisboa, Lisboa, Portugal vale.filipa@gmail.com
5 National Reference Laboratory for Gastrointestinal Infections, Department of Infectious Diseases, National Institute of Health Dr Ricardo Jorge, Lisboa, Portugal. Monica.Oleastro@insa.min-saude.pt
6 Department of Microbiology, Hospital Universitario La Princesa, Instituto de Investigación Sanitaria Princesa, Madrid, Spain, talarcon@helicobacterspain.com
7 Division of Gastroenterology, Rabin Medical Center, Petah Tikva, Israel, tzahipe1@clalit.org.il
8 Department of Biology, Faculty of Sciences, University of Mohaghegh Ardabili, Iran, s_latifi@uma.ac.ir
9 Department of Environmental and Preventive Medicine, Oita University Faculty of Medicine, Yufu, Oita, Japan yyamaoka@oita-u.ac.jp
10 Laboratory of Medical Microbiology, Hellenic Pasteur Institute, Greece, bmartinez@pasteur.gr, y.karayiannis@hotmail.com, tkaram@pasteur.gr, sgouras@pasteur.gr
11 G42 Healthcare; Abu Dhabi, wfmelamin@yahoo.com
12 Elrazi University; Khartoum; Sudan
13 The Milner Centre for Evolution, Department of Biology and Biochemistry, University of Bath, Claverton Down, Bath, UK, bp467@bath.ac.uk, sks70@bath.ac.uk
14 Center for Life Course Health Research, University of Oulu;
15 Primary Health Care Center, Tornio, Finland jukka.ronkainen@fimnet.fi
16 Arokero Oy, Tornio, Finland. pertti.aro@fimnet.fi
17 Center for Translational Microbiome Research, Department for Microbiology, Tumor, and Cell Biology, Karolinska Institutet, Stockholm, Sweden, lars.engstrand@ki.se
18 Division of Family Medicine, Karolinska Institutet, Stockholm, Sweden, lars.agreus@ki.se

41 19 Department of Medical Microbiology and Hospital Epidemiology, Max von Pettenkofer
42 Institute, Faculty of Medicine, LMU Munich, Munich, Germany, suerbaum@mvp.lmu.de
43 20 Department of Medical Microbiology and Hospital Epidemiology, Hannover Medical
44 School, Hannover, Germany
45 21 DZIF German Center for Infection Research, Hannover-Braunschweig and Munich Partner
46 Sites, Germany
47 22 Institute of Biomedicine, Department of Infectious Diseases, University of Gothenburg,
48 Gothenburg, Sweden. Kaisa.thorell@gu.se
49 23 Department of Clinical Microbiology, Sahlgrenska University Hospital, Gothenburg,
50 Sweden
51 & Contributed equally.
52 § Shared senior authors
53 * Corresponding author: Daniel Falush, danielfalush@googlemail.com

Abstract

Helicobacter pylori lives in the human stomach and has a population structure which resembles that of its host. However, *H. pylori* from Europe and the Middle East trace a substantially higher fraction of ancestry from modern African populations than the humans that carry them. Here, we used a collection of Afro-Eurasian *H. pylori* genomes to show that this African ancestry is due to at least three distinct admixture events. *H. pylori* from East Asia, which have undergone little admixture, have accumulated many more non-synonymous mutations than African strains. European and Middle Eastern bacteria have elevated African ancestry at the sites of these mutations compared to either non-segregating or synonymous sites, implying selection to remove them. We used simulations to show that demographic bottlenecks can lead to long-term segregation of deleterious mutations, despite high rates of homologous recombination, but that population fitness can be restored by migration of small numbers of bacteria from non-bottlenecked populations, leading to mosaic patterns of ancestry like that seen for *H. pylori*. We conclude that *H. pylori* have been able to spread repeatedly from Africa by outcompeting strains that carried deleterious mutations accumulated during the original out-of-Africa bottleneck.

Main text

Introduction

Helicobacter pylori is the dominant bacterial member of the human stomach microbiota in infected individuals and is the aetiological agent in most cases of gastric cancer, gastric mucosa-associated lymphoid tissue (MALT) lymphoma, and gastroduodenal ulcer disease [1]. *H. pylori* causes chronic, decades-long infections and is often acquired within the household, limiting the rate of its diffusion through human populations in comparison with more readily transmissible pathogens [2]. Genetic variation in *H. pylori* genome sequences shows a phylogeographic pattern similar to that of its host, consistent with an inference that human and bacterial genes are often spread by the same migrations[3-6] . However, the *H. pylori* population found in Europe and other parts of Eurasia is admixed, with many strains having more than half of their DNA attributable to populations closely related to those prevalent in Africa [3,7-9]. There is evidence for several recent human migrations out of Africa[10], but together they have only contributed a small fraction of the ancestry of non-Africans. This discrepancy in ancestry proportions between the bacteria and their hosts implies that African *H. pylori* has been spread to Eurasia by movements of people that have left weaker signals in human DNA.

To understand why African *H. pylori* have contributed extensive ancestry within parts of Eurasia, we have assembled a collection of strains from Europe and the Middle East, from putative source populations in Africa, as well as from less-admixed strains in Asia. We infer a recent demographic history of the European and Middle Eastern strains that includes genetic drift, migration, and admixture from external sources. We show that there have been at least three admixture events from African source populations that have each

contributed substantial ancestry. By examining the distribution of non-synonymous mutations in different populations, we conclude that there was a large and lasting increase in the frequency of segregating deleterious mutations during the out-of-Africa bottleneck associated with the initial spread of modern humans from Africa. When African *H. pylori* strains reached Eurasia due to later contact between humans, they, and the DNA they carried, had a fitness advantage and were able to spread. In the process, they reduced the mutational load in the newly admixed populations.

Repeated African Admixture into Europe and the Middle East

Based on fineSTRUCTURE clustering (Figure S1), we grouped European and Middle Eastern strains into four subpopulations named hspEuropeNEurope, hspEuropeCEurope, hspEuropeSWEurope and hspEuropeMiddleEast according to the locations they were most isolated from. The first Europe in the name indicates they are subpopulations of hpEurope but for brevity we omit this part of the name in the rest of the manuscript. We investigated their sources of external ancestry by performing *in silico* chromosome painting (Figure 1A) using donor strains from three African populations (hspENEAfrica, hspCNEAfrica, hspAfrica1WAfrica) and two Asian populations (hpAsia2 and hspEAsia). Representative strains from these populations were selected from a larger collection on the basis that they showed little sign of recent admixture from other continents based on D-statistics (Table S5,S6) and as confirmed in a PCA plot (Figure S2).

The chromosome painting analysis supported previous findings that there is a North-South cline in the overall proportion of African ancestry and that hpAsia2 is a closer relative of the pre-admixture population than hspEAsia[3,8]. However, all isolates are painted with a substantial and largely consistent fraction of hspEAsia (with the hpAsia2:hspEAsia ratio varying from 1:1.74 for hspNEurope to 1:2.02 for hspMiddleEast), implying that hpAsia2 is not a close surrogate for the pre-admixture population.

To investigate the demographic history of admixture further, we measured genetic drift profiles separately for each ancestry component (Figure 1B). Specifically, we compared the painting profile of pairs of admixed individuals to identify regions of the genome in which they were painted by the same donor population. For these genomic regions, we recorded if they were painted by the same specific donor strain (Methods). High rates of painting by the same donor strain indicates shared genetic drift within that ancestry component. These values are similar in interpretation to F3 values[11], but are specific to individual ancestry components, rather than averaged across the entire genome.

Genetic drift profiles for the hpAsia2 and hspEAsia ancestry components showed a similar pattern across the four hpEurope subpopulations, as indicated by near identical pattern of colours for these two ancestry components in Figure 1B. The indistinguishable drift profiles provide evidence that within each hpEurope subpopulation, both components have been affected similarly by genetic drift. The simplest explanation is that these components are both being used to paint a single ancestry source that persisted in western Eurasia since the

out-of-Africa bottleneck. Therefore, the data does not provide evidence for either ancient or more modern genetic contributions from the East.

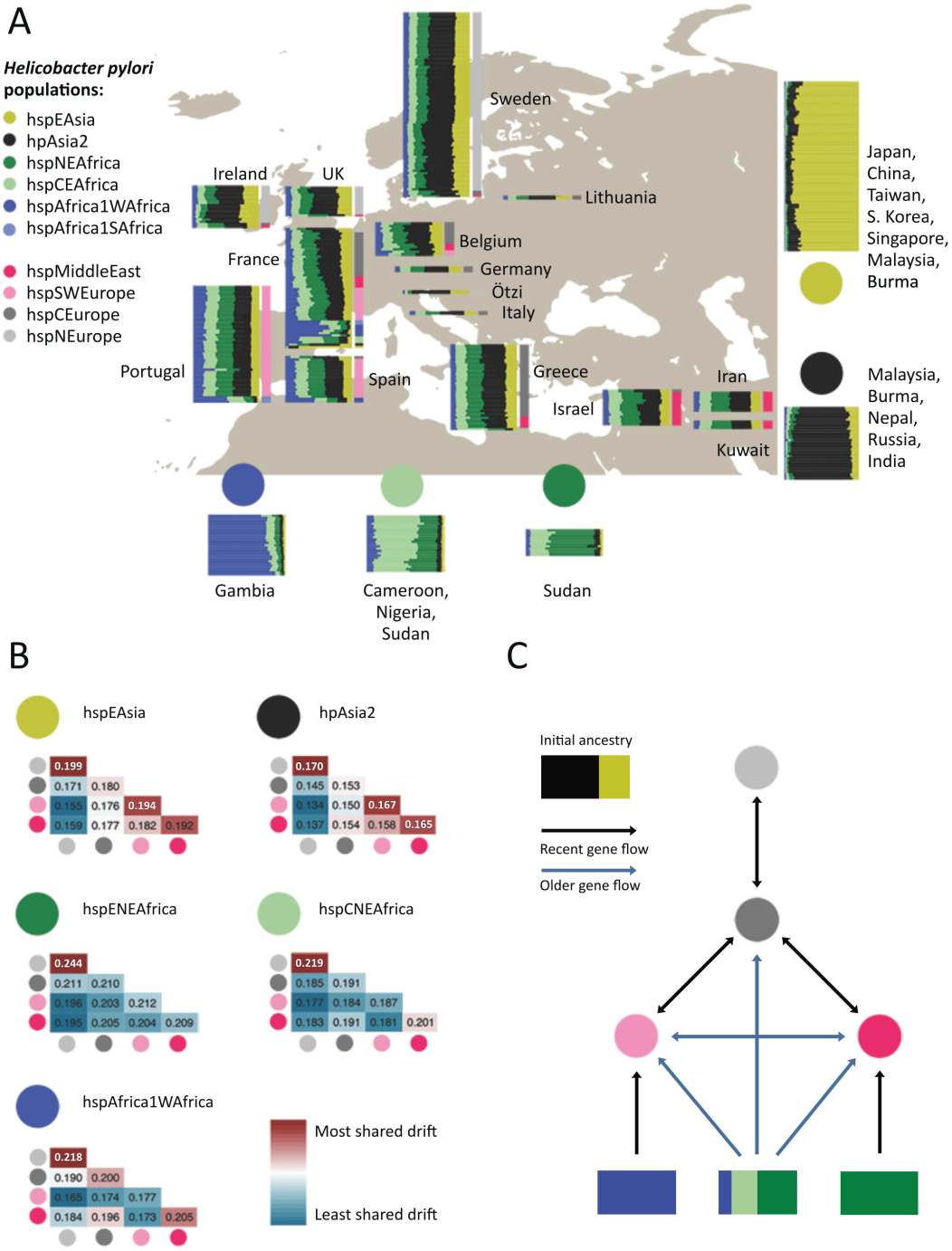

Figure 1 *Ancestry and migration history of hpEurope isolates. (A) Painting profiles of hpEurope isolates and their putative ancestral populations from Africa and Asia showing proportion of each genome (horizontal bar) painted by each of five ancestral donor populations (circles). hpEurope isolates are grouped by country of isolation, with bars to the right indicating the H. pylori population each strain is assigned to. The representative*

isolates from each donor population are grouped by population, with countries of isolation listed for each group. (B) Genetic drift profiles for hpEurope subpopulations, shown separately for each ancestry component. (C) Schematic summarizing the migration and admixture history of the hpEurope subpopulations.

In addition to the North-South cline, there is also an East-West ancestry cline in the source of African admixture (Figure 1A), with distinct drift patterns for each African component in the four hpEurope subpopulations (Figure 1B). Strains from hspSWEurope have the highest fractions of hspAfrica1WAfrica and this ancestry component shows low levels of drift, implying that this subpopulation has undergone recent admixture from strains closely related to those currently found in West Africa. Furthermore, there are strains from Spain, Portugal and France assigned to hspAfrica1 subpopulations and a strain in Portugal with an intermediate ancestry profile suggesting that these isolates have arrived within the last few human generations. Strains from the hspMiddleEast subpopulation have the highest fraction from hspENEAfrica and the lowest levels of drift in this component. These two populations have therefore received genetic material from Africa after the initial gene flow that has introduced ancestry across the continent. These patterns imply that there have been at least three separate admixture events involving distinct populations of African bacteria (Figure 1C). Confirmation of these results is provided by an admixture graph estimated by Treemix [12] (Figure S3). Treemix estimated nine migration events across the 11 populations in this study, three of which were from Africa into the European sub-populations. These three events corresponded closely to the three events found using chromosome painting.

The drift components also provided evidence about local migration. hspMiddleEast and hspSWEurope have high levels of shared drift in both Asian components, implying that prior to admixture, these two populations were closely related. hspNEurope has high subpopulation-specific drift in all ancestry components, showing that it has undergone recent genetic drift, while hspCEurope has almost none in any component, suggesting that it has been a hub for migration between populations.

The genome of a strain colonizing the Tirolean iceman, Ötzi, has been inferred to be a nearly pure representative of the pre-admixture population based on more limited data, which was interpreted as evidence that most of the admixture took place in the 5,300 years since his death [8]. In our fineSTRUCTURE analysis, the Ötzi genome clusters with hspNEurope isolates from Ireland and Sweden with the lowest African ancestry, one of which has the same non-African ancestry proportion as the Ötzi strain in the chromosome painting. These results show that the Ötzi genome, in fact, falls within modern variation in ancestry proportions in Europe. We interpret this as evidence that substantial African ancestry had already been introduced into Europe when Ötzi lived but that ancestry proportions in particular locations have changed substantially in subsequent millennia.

Overall, the chromosome painting results show that, in addition to contemporary migrations that have introduced *H. pylori* with atypical profiles into countries such as Ireland, Portugal, France and Spain (Figure 1A), *H. pylori* have spread out of Africa at least three times (Figure 1C). Each of these migrations is sufficiently old that the DNA has been absorbed into the local gene pools, leading to a high degree of uniformity in ancestry profiles for most isolates in individual locations (Figure 1A). At least one of the early admixture events was shared between the four subpopulations, spanning Europe and the Middle East, and left traces in Ötzi's *H. pylori* genome, while later ones, labelled as "recent" in Figure 1C, had foci in South Europe and the Middle East, respectively. Gene flow between the regional subpopulations has affected all ancestry components but has not been sufficient to homogenize ancestry proportions across the continent.

Evidence for a role of deleterious mutations in the repeated expansion of bacteria from Africa.

The ability of *H. pylori* of African origin to spread effectively in non-African populations on multiple independent occasions is unexpected, since the resident bacteria will have had an opportunity to adapt to local conditions. One potential explanation is that deleterious mutations accumulated in the genomes of strains carried by the early waves of modern humans that spread from Africa. Demographic bottlenecks associated with these migrations have been sufficient to leave an imprint on neutral genetic variation within the human genome, which indicate a reduction in effective population size in the ancestry of non-African humans around 50,000 years ago, followed by more recent expansion[13]. *H. pylori* populations also show evidence of low ancestral population sizes in East-Asian and native American populations, followed by population size recoveries[6] consistent with strong genetic drift during the out-of-Africa and subsequent bottlenecks.

Population genetic theory [14] and evidence from experimental systems [15] has shown that demographic bottlenecks can lead to reduction in average fitness through processes such as fixation of deleterious mutations of small effect or the stochastic loss of the fittest genomes (Muller's ratchet [16,17]). However, although the out-of-Africa bottlenecks have had measurable impact on the pattern of segregating mutations within human populations [18], there is less evidence that individuals from non-African populations have accumulated a larger burden of non-synonymous mutations when measured relative to an outgroup[19]. *H. pylori* shows much higher rates of genetic differentiation between geographical regions [4] than its host [13], which most likely reflects transmission bottlenecks during spread from person to person as well as the expansion of fit clones. Consequently, demographic bottlenecks that have had modest fitness consequences for humans can potentially have more substantial effects on the bacteria they carry.

227 Bacteria from the hspEAsia and hpAsia2 populations, which have been through the out-of-
228 Africa bottleneck, had a higher number of deleterious mutations segregating between
229 strains (Figure 2A) and a higher dN/dS to the *H. acinonychis* outgroup (Figure 2B, S4B) than
230 do the three African populations with comparable synonymous divergence levels dS. dN/dS
231 for the three African populations ranged between 0.137 and 0.138, with Asian populations
232 having values of 0.140 and 0.141. This corresponded to an average of 574 extra non-
233 synonymous mutations in the Asian populations or 1 mutation for every 3 genes. dN/dS
234 values within populations varied between 0.123-0.133 for African populations and 0.163-
235 0.169 for the Asian ones. This difference corresponded to an average of 1216 non-
236 synonymous differences between pairs of strains or about 2/3 of a SNP per gene. These
237 results show that the larger number of differences in dN/dS to the outgroup in the Asian
238 populations reflects a larger number of segregating non-synonymous variants and thus
239 cannot simply be attributed to fixation of mutations during the out-of-Africa bottleneck.
240
241 We confirmed the robustness of these results in two ways. Firstly, we used GRAPES [20] to
242 estimate the rate of non-adaptive non-synonymous substitutions based on the pattern of
243 segregating mutations within each population. This approach can be applied with a folded-
244 mutation spectrum, obviating the need for an outgroup. The results were highly concordant
245 with those obtained for dN/dS values (Figure S5). Secondly, when an hpAfrica2 strain was
246 used as an outgroup instead of *H. acinonychis*, similar results were obtained for dN/dS, but
247 the range of dS values between populations was twice as large (Figure S6). This suggested
248 that there have been ancient admixture events involving Africa2-like lineages and other
249 African populations, while confirming the higher mutation load in Asian populations.
250

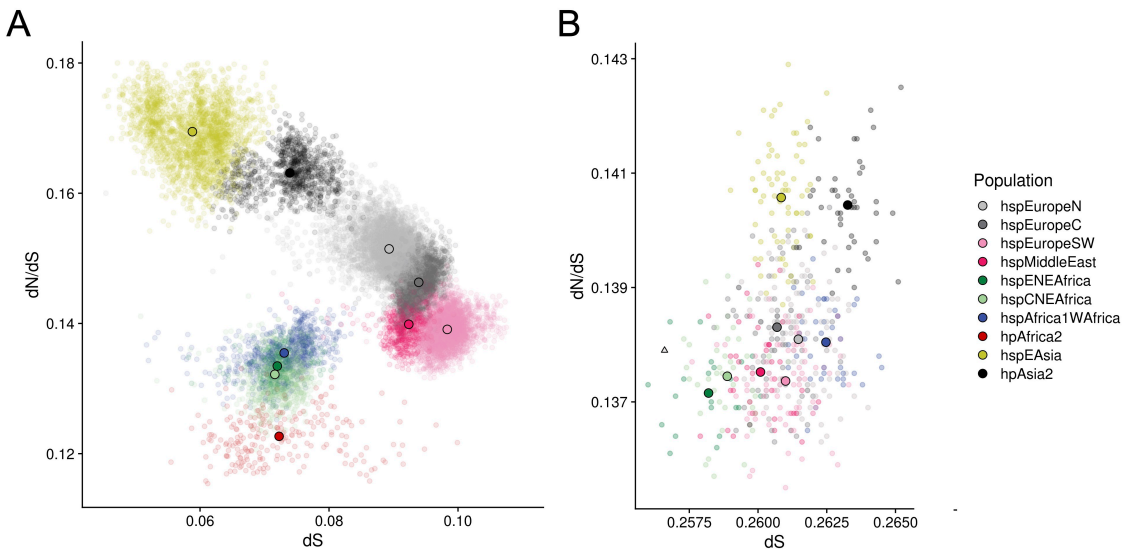

251
252 ***Figure 2*** *Within- and between-population divergence. (A) Within population dN/dS (y axis)*
253 *plotted against dS (x axis). Small dots show pairwise distances; larger solid dots indicate*
254 *population means. (B) dN/dS, calculated to the H. acinonychis outgroup, plotted against dS*

for isolates (semi opaque points) and populations (solid points), excluding hpAfrica2 isolates. The triangle indicates the genome from Ötzi.

We also observed a reduction of the mutational load by admixture and selection within hpEurope subpopulations. Bacteria from hpEurope subpopulations had dN/dS values with the *H. acinonychis* outgroup that were intermediate between African and Asian populations but were lower (0.137-0.138) than would be predicted if they were random mixtures of African and Asian genomes with the proportions estimated by chromosome painting in Figure 1A (0.139-0.140). However, this mutation deficit is not on its own compelling evidence for a direct benefit of admixture, since it might instead reflect differences in dN/dS between the population that existed in Europe prior to admixture and the Asian populations that were used as surrogates for this ancestry in this analysis.

More specific evidence that admixture has reduced the burden of deleterious non-synonymous mutations was provided by tabulating the effect of mutations that accumulated in African and Asian populations on the ancestry of admixed bacteria in Europe and the Middle East (Figure 3). For each position in the alignment, we calculated a mutation score, which is the difference between African and Asian strains in the proportion of nucleotides that differed from *H. acinonychis* (with equal weight given to each subpopulation, see methods). We then investigated whether there is variation in overall Asian ancestry proportion (hpAsia2+hspEAsia in the chromosome painting) associated with this score. Most sites were non-polymorphic and had a mutation score of 0.0, which was therefore used as a baseline and compared independently to positive and negative scoring sites. To allow for correlations between adjacent sites, statistical significance of the regression was assessed using a gene-by-gene jackknife (methods).

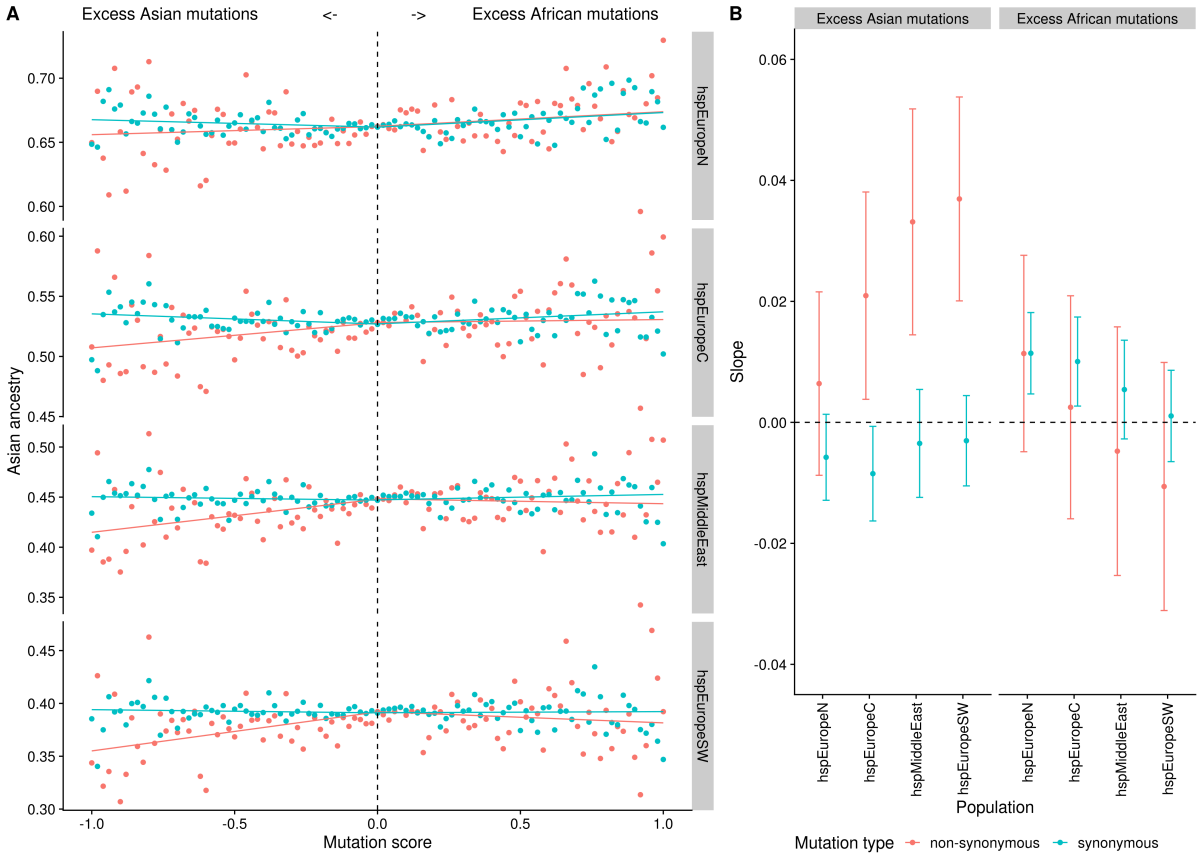

Figure 3 *Genetic ancestry of hpEurope subpopulations as a function of mutation score. (A) Average ancestry in chromosome painting analyses plotted against mutation score (mutation frequency in African populations minus mutation frequency in Asian populations) in bins of 0.02. Regression lines were calculated separately for positive and negative mutation scores. (B) Regression slopes with 95% confidence intervals estimated using a gene-by-gene jackknife for excess Asian and excess African mutations, respectively.*

H. pylori shows little evidence for codon usage bias[21], so most synonymous mutations should be approximately neutral and can therefore be used as a control. A negative mutation score at non-synonymous sites is associated with a deficit in Asian ancestry, either in comparison with non-polymorphic sites or with synonymous sites with the same scores. The strongest regression slopes were estimated for the two Southern populations, and the weakest estimated for hspNEurope (Figure 3A,B). By contrast, excess mutations in African strains did not have a detectable effect on ancestry in any of the four hpEurope subpopulations, with regression slopes statistically indistinguishable from those found for synonymous positions. Thus, admixed bacteria have avoided non-synonymous mutations that accumulated in populations that have been through the out-of-Africa bottleneck, but not those that have not. We inferred that a proportion of these non-synonymous mutations are deleterious and have been selected against in the admixed population. Similar results were obtained, albeit with lower statistical confidence, when an hpAfrica2 strain was used as an outgroup instead of *H. achinonychis* (Figure S7A,B).

Deleterious mutations occurred throughout the genome and were all subject to genetic drift. A plot of mutation score versus ancestry at a gene-by-gene level showed considerable scatter (Figure S8A, Table S7), with similar results obtained when the analysis was performed for 10kb regions (Figure S8B), suggesting that the signal that we observed for mutation replacement cannot be attributed to a small number of genes. Nevertheless, it is possible that other selective forces, for example related to local adaptation, could explain some of the variation in ancestry proportion between genes.

We investigated whether specific genes were enriched for African ancestry. There was substantial variation amongst genes in the average African ancestry proportion, with strong correlations between proportions in the four hpEurope subpopulations (Figure S9), which is consistent with much of the ancestry resulting from a single shared admixture event. However, we observed no significant differences between COG categories in average ancestry proportion (Figure S10).

Genes with extreme values of average ancestry proportion were involved in diverse, often central, cellular processes. For example, low African ancestry (top ten in Table S7, each with <27% average African ancestry) genes included, *e.g.*, those in central energy generation (HP0145, component of the Cbb3-type terminal oxidase), stress tolerance (HP0278, *ppx* exo-polyphosphatase; HP0600, *spaB* multidrug resistance), cell envelope biogenesis (HP0867, lipid A), and translation (HP1147, ribosomal proteins L19). However, the analysis did reveal overlap of low-admixture genes with genes that have highly differentiated SNPs within East Asia [22], specifically HP0284 (*mscS-1*), encoding a mechanosensitive channel related to osmo-tolerance and HP0250 (*oppD*), encoding an oligopeptide permease. Since the same genes are often differentiated in different continents [22], this overlap suggests that these genes may have been resistant to admixture due to local adaptation within Europe and the Middle East.

High-average African ancestry genes (>69%) likewise included those in central biological processes and stress tolerance, such as those of the Czc cation efflux system (HP0969-HP0970, metal ion tolerance and nickel homeostasis), purine salvage (HP0267, cytosine/adenine deaminase), and glycolysis (HP1166, glucose-6-phosphate isomerase & HP0154, enolase). Most were not directly related to host interactions, although some with low average African ancestry might affect urease activity (HP1129, *exbD* & HP0969-HP0970, *czc*). Overall, this inspection supported that the driving force for admixture within the core genome was increased fitness, provided by replacement of stochastic deleterious mutations genome-wide, rather than single pathogenesis-related genes allowing adaptation to new host environments.

To test the hypothesis that selection on deleterious mutations can explain the observed patterns, we performed simulations of bacterial populations evolving with a constant input of neutral and deleterious mutations and homologous recombination of short tracts (Figure 4, Figure S11,S12). These simulations showed that at high recombination rates,

demographic bottlenecks could generate long-term increases in the number of deleterious mutations segregating in the population (Figure 4A, Figure S12C,D), and in dN/dS measured relative to an outgroup (Figure 4B, Figure S12E,F). These patterns qualitatively match those seen in the data (Figure 2A,B).

In our simulations, the average fitness of the bottlenecked population underwent the largest decrease at intermediate recombination rates (Figure 4C, Figure S12A,B) and in this simulation, the bottlenecked population was susceptible to invasion from strains from the non-bottlenecked population. Once an invading strain became established in the non-bottlenecked population, the frequency of migrant DNA increased in an almost stepwise fashion leading to the generation of highly mosaic genomes (Figure 4D,E). As migrant DNA spread through the population, mutations from the bottlenecked population that were deleterious fell faster in frequency than mutations at neutral sites (Figure 4F) reproducing the dependence observed in the data (Figure 3A). This showed that the interplay between recombination and selection can explain the reduced mutational burden of the admixed populations.

Our simulations are consistent with results obtained for eukaryotic systems, which have shown that population bottlenecks can increase mutational load [23] and that gene flow from populations with a higher effective population size to those with a smaller one decreases the genetic load of the smaller population [24]. This effect is particularly strong in regions of higher recombination, for which introgressed neutral/beneficial mutations will persist due to their uncoupling with the introgressed deleterious mutations. However, our simulations show that for bacterial populations the decrease of the genetic load due to admixture is only valid for intermediate recombination levels. For higher recombination rates, admixture has no effect on the fitness of the smaller population, since selection is already effective in removing deleterious mutations.

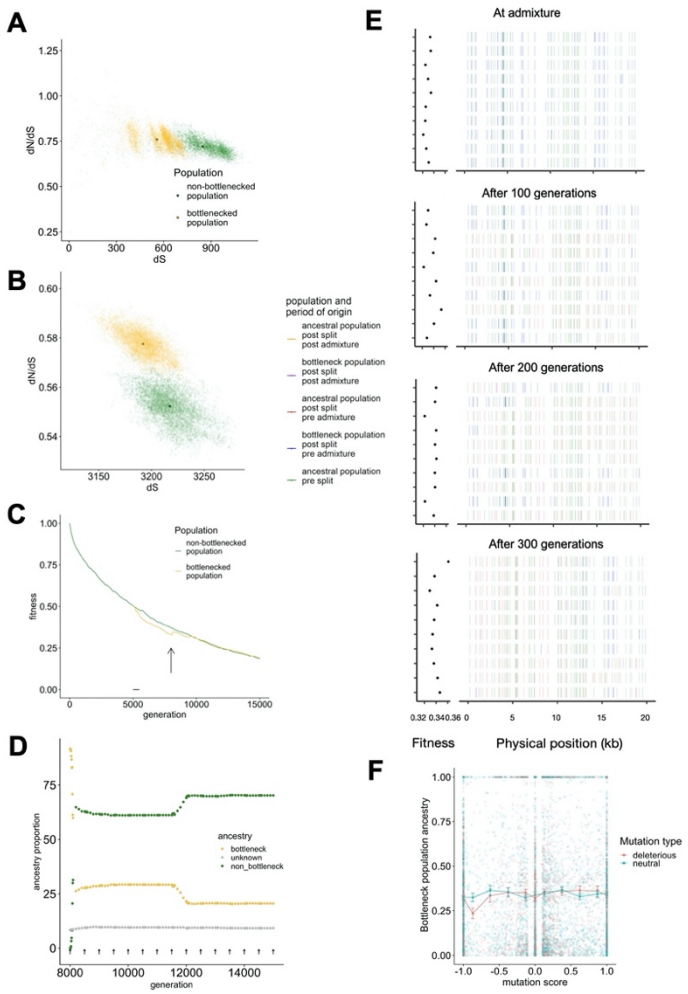

Figure 4. *Simulations of populations under bottlenecks and admixture. (A) Within population dN/dS and (B) dN/dS calculated to the ancestor measured at generation 8000. Semi opaque points show pairwise distances; solid points indicate population means. (C) Population average fitness shown during the generations of the simulation, with bottleneck starting at generation 5000 and admixture at generation 8000, with each arrow corresponding to the migration of a single strain. (D) Proportion of bottleneck and non-bottleneck ancestry in the bottleneck population, for the generations after the beginning of admixture. Sites with unknow ancestry are shown in grey. Each arrow corresponds to the migration of one strain. (E) Ancestry painting in a sample of genomes from the bottleneck population, in the generations subsequent to admixture. Only the first 20kb of each genome is shown. (F) Average bottleneck population ancestry, at generation 8300 plotted against mutation score (frequency in the non-bottleneck population minus the frequency in the bottleneck population before the admixture begins).*

Discussion

Deleterious mutations provide a compelling explanation for the repeated spread of African *H. pylori* into other continents, as shown by the good qualitative match between our simulation results and the pattern of diversity within contemporary *H. pylori* populations.

396 First, we find elevated dN/dS values in Asian populations, consistent with a higher load of
397 deleterious mutations accumulating during the out-of-Africa bottleneck. Secondly, our
398 simulations show that rare migrants from non-bottlenecked populations can spread and
399 generate highly mosaic genomes, as observed in Europe and the Middle East. Third we show
400 that ancestry from these invading lineages is higher in regions of the genome where non-
401 synonymous mutations are segregating within the bottlenecked populations, implying that
402 selection has acted to purge these mutations during admixture.
403
404 Deleterious mutations have been shown to be important during hybridization in several
405 eukaryotic systems, including swordfish [26], trees [27] and Neanderthal introgression into
406 modern humans[25]. In these systems, recombination rate variation has been shown to be
407 crucial in determining the rate of introgression that has taken place in different regions of
408 the genomes. To our knowledge, this is the first demonstration of a load effect in bacteria.
409 *H. pylori* is known to recombine at an extraordinary rate [28-30] and this may explain why a
410 clear signal is observable in this species.
411
412 Many of the details concerning the spread of African ancestry remain to be elucidated. The
413 initial admixture event(s) left traces in the *H. pylori* genome of the Tirolian Iceman
414 Ötzi, which has an ancestry profile like that found in modern day samples in Ireland and
415 Sweden but has less African ancestry than in modern genomes from Southern Europe.
416 Therefore, the first admixture event occurred more than 5300 years ago but the average
417 level of African ancestry has increased substantially in the last few millennia.
418
419 *H. pylori* of different origins can mix together and recombine within extended families[31].
420 Over time, extensive ongoing contacts between populations within Europe would be
421 expected to homogenize *H. pylori* ancestry proportions both within and between locations.
422 However, we lack quantitative information on transmission dynamics that might allow us to
423 estimate mixture dates based on the properties of the ancestry clines we observe.
424
425 An intriguing question is why some populations appear to have been resistant to invasion by
426 DNA from African *H. pylori*. For example, within East Asia, most strains appear to come from
427 the hpEAsia population, with very little evidence of admixture. Lack of contact with Africans
428 does not seem a sufficient explanation, given the large number of documented contacts
429 between East Asians and other Eurasian populations within the last several thousand years.
430 The high burden of *H. pylori* related gastric disease in the region is notorious and hpEAsia
431 bacteria are known for distinctive variants at virulence associated loci including *cagA* and
432 *vacA*[32]. It is possible that strains from this population have acquired a suite of adaptations
433 that allows them to outcompete invading bacteria despite the large mutation load within
434 their genomes. This raises the possibility that some of the non-synonymous mutations that
435 rose to high frequency during the bottleneck may have allowed rapid adaptation, in other
436 words a form of evolution by shifting balance[33].
437

438 *H. pylori* seems to be an outlier amongst bacteria in many features of its biology [30], including
439 its slow rate of spread between human populations and its high mutation [28] and
440 recombination rates [29]. Our results suggest that recombination may save strains from rapid
441 mutational meltdown but that deleterious mutations persist within populations, with the
442 effects of bottlenecks enduring for millennia. The unusual properties of *H. pylori* make it a
443 powerful model system for understanding how deleterious mutations interact with
444 demographic processes and adaptive ones to mould diversity within natural populations.
445
446
447 **Methods**
448 ***Dataset collection***
449 A dataset of 716 *Helicobacter pylori* whole-genome sequences was assembled, consisting of
450 213 newly sequenced isolates from Europe, Asia and Africa (Table S1) and selected publicly
451 available genomes (Table S2).
452
453 ***Genome sequencing***
454 New genomes were sequenced at five different centres: Karolinska Institute, Sweden (KI),
455 Hannover Medical School, Hannover, Germany (MHH), Hellenic Pasteur Institute, Greece
456 (HPI), Oita University, Japan (OiU), and University of Bath, UK (UBa) (Table S1).
457
458 Genomic DNA from strains marked with KI in Table S1 was extracted using DNeasy Mini Kit
459 (Qiagen, Hilden, Germany) following the manufacturer's guidelines for Gram-negative
460 bacteria. Sequencing libraries were prepared using the TruSeq Nano kit (Illumina, San Diego,
461 CA, USA) and sequenced on the MiSeq platform, v3 chemistry, using 300 bp paired end
462 mode.
463
464 Genomic DNA from strains marked MHH was isolated from *H. pylori* strains after 24h culture
465 on *H. pylori* selective agar (in-house recipe) with the Genomic Tip 100/G (Qiagen, Hilden,
466 Germany). Nextera XT libraries were generated and sequenced in three different runs on
467 MiSeq 2x300bp paired (Illumina, San Diego, CA, USA), as recommended by the
468 manufacturer. All quantification steps of gDNA and NGS libraries were done with Qubit
469 dsDNA HS Assay Kit (Invitrogen, ThermoFisher Scientific, Carlsbad, CA, USA).
470
471 For strains marked with HPI, adapter-compatible DNA was prepared using Ion Xpress™ Plus
472 Fragment Library Kit and enzymatically fragmented for 5-12 minutes, resulting in a median
473 fragment size of 350-450 bp and the libraries were prepared using the Ion Plus Fragment
474 Library Kit. The resulting 400 bp insert libraries were used to prepare enriched, template-
475 positive Ion PGM™ Hi-Q™ View Ion Sphere Particles (ISPs) with the Ion OneTouch™ 2
476 System. 850-flows sequencing was performed using the Ion PGM™ Hi-Q™ View Sequencing
477 Kit with the Ion 318™ Chip Kit v2.
478

479 For genomes marked with UBa, genomic DNA was quantified using a NanoDrop
480 spectrophotometer, as well as the Quant-iT DNA Assay Kit (Life Technologies, Paisley, UK)
481 before sequencing. High-throughput genome sequencing was performed using a HiSeq 2500
482 machine (Illumina, San Diego, CA, USA).
483
484 Genomic DNA from strains marked with OiU was extracted using DNeasy Blood & Tissue kit
485 (QIAGEN, Hilden, Germany). DNA concentration was measured using QuantusTM
486 Fluorometer (Promega). High-throughput genome sequencing was performed either on
487 Hiseq 2000 (2 × 100 or 2 × 150 paired-end reads) or Miseq (2 × 300 paired-end reads)
488 sequencer (Illumina, San Diego, CA) following the manufacturer 's instruction.
489
490 ***Primary bioinformatics analysis***
491 For the KI genomes, the raw sequencing reads were quality trimmed and filtered using
492 TrimGalore! (http://www.bioinformatics.babraham.ac.uk/projects/trim_galore/) applying a
493 minimum q-score of 30, and *de novo* assembled using SPAdes [34] with the –careful option.
494 Contigs with very low coverage and that were shorter than 500 bp were discarded prior to
495 annotation.
496
497 For the MHH genomes quality filtering was done with Trimmomatic version 0.36 [35] and the
498 assemblies were performed with SPAdes genome assembler v. 3.9.0 and resulted in number
499 of all contigs from 26 up to 117. Assemblies were quality controlled with QUAST[36].
500
501 For the HPI genomes, quality control of raw sequencing reads was performed using FASTQC
502 (https://www.bioinformatics.babraham.ac.uk/projects/fastqc). Unbiased *de novo* assembly
503 was performed using SPAdes genome assembler v.3.5.0in default mode.
504
505 For the UBa genomes, raw sequencing reads were quality trimmed and filtered using
506 Trimmomatic version 0.33 and the 100 bp short read paired-end data was assembled using
507 the *de novo* assembly algorithm Velvet version 1.2.08[37]. The VelvetOptimiser script (version
508 2.2.4) was run for all odd k-mer values from 21 to 99. The minimum output contig size was
509 set to 200 bp with default settings, and the scaffolding option was disabled.
510
511 For the OiU genomes, Trimmomatic v0.35 was used to remove adapter sequences and low-
512 quality bases from raw short reads data. Trimmed reads were then de novo assembled to
513 produce contigs using SPAdes genome assembler v3.12.0 with the -careful option to reduce
514 mismatches in the assembly. The minimum contig length was set to 200 bp.
515
516 Annotation of both newly sequenced draft genomes and publicly available sequences was
517 performed using the prokka annotation pipeline v 1.12 [38] using the most recent version of
518 the 26695 genome [39] as primary annotation source.

519 Genome size and contig/scaffold number was collected from the prokka annotation output
520 using the MultiQC tool [40] and collected into Table S3 . All newly sequenced genomes were
521 submitted to GenBank under BioProject PRJNA479414.
522 All strains, their population designations and their role in the respective analyses are shown
523 in Table S4.
524
525 ***Sequence comparison and alignment:***
526 All isolates were mapped to the 26695 genome (NC000915.1) using the Snippy software
527 version 3.2-dev (https://github.com/tseemann/snippy). The resulting core genome, which
528 was collected with the same tool, contained 287 746 core SNPs from 979 771 variant sites.
529
530 ***FineSTRUCTURE***
531 We inferred population structure among the strains based on the genome-wide haplotype
532 data of the reference-based alignment to 26695 described above, using chromosome
533 painting and fineSTRUCTURE [41] according to a procedure of our preceding study that applied
534 them to *H. pylori* genome[42]. Briefly, we used ChromoPainter (version 0.04) to infer chunks of
535 DNA donated from a donor to a recipient for each recipient haplotype and summarized the
536 results into a "co-ancestry matrix", which contains the number of recombination-derived
537 chunks from each donor to each recipient individual. We then ran fineSTRUCTURE (version
538 0.02) for 100,000 iterations of both the burn-in and Markov Chain Monte Carlo (MCMC)
539 chain, in order to conduct clustering of individuals based on the co-ancestry matrix.
540
541 ***Choice of donor and recipient strains and chromosome painting***
542 D-statistics were calculated for strains assigned to each of the five ancestral populations
543 hspEAsia, hpAsia2, hspCNEAfrica, hspENEAfrica and hspAfrica1WAfrica. D-statistics were
544 calculated using popstats (https://github.com/pontussk/popstats) and specifying individual
545 A as SouthAfrica7 (hpAfrica2), individual B as GAM260Bi (hspAfrica1WAfrica), individual Y as
546 F227 (hspEAsia) and individual X. In this comparison, negative D-statistics imply more
547 African ancestry in the strain designated as individual X than in F227. D-statistics values can
548 be found in Table S5 and Table S6.
549
550 A subset of strains from each of the five ancestral populations were chosen as donors to get
551 groups of similar size and were selected based on the fineSTRUCTURE analysis to get good
552 representativeness over the donor populations. Some hpAsia2 strains showed signs of
553 elevated African admixture based on negative D-statistics values and these strains were not
554 selected as donors.
555
556 We conducted chromosome painting of 646 recipient strains (belonging to hspNEurope,
557 hspCEurope, hspSWEurope, hspMiddleEast, hspENEAfrica, hspEAsia, hspCNEAfrica,
558 hspAfrica1WAfrica, hpAsia2, and hpAfrica2). For this purpose, we used ChromoPainterV2
559 software [41]. For each recipient population, we calculated site-by-site average copying

560 probability from each of the five donor populations. Gene-by-gene averages were also
561 calculated by averaging of the sites in each gene for the 790 genes in the alignment.
562 Regressions between gene-by-gene averages in different hpEurope subpopulation were
563 calculated using the aq.plot() function in R.
564
565 ***Shared drift estimation***
566 We used the chromosome painting analysis to investigate shared genetic drift profiles. We
567 calculated a separate drift profile for each pair of hpEurope subpopulations, including a
568 within-population profile. For each profile, we calculated separate drift values for each of
569 the five ancestry components (with the components shown in separate triangles in Figure
570 1B). For example, to calculate the shared drift profile of hspNEurope and hspSWEurope, we
571 took each combination of pairs of strains from the two populations and asked whether they
572 used donors from the same population at each site in the genome. We also tabulated
573 whether they used exactly the same donor strain. The drift value for that pair of populations
574 for that ancestry component is the ratio of shared donor to shared strain, summed over all
575 pairs and sites in the genome.
576
577 **dN/dS calculations**
578 From the fineSTRUCTURE analysis, a sub-dataset was collected consisting of the European
579 strains assigned to the hpEurope populations, together with a representative selection of
580 strains from the ancestral populations hpAfrica2, hspAfrica1WAfrica, hspCNEAfrica,
581 hspENEAfrica, hpAsia2, and hspEAsia. The *H. acinonychis* genome was added to this dataset
582 to provide an outgroup. For a detailed list of which strains that were included in these
583 analyses, see columns in Table S2,S4. dN/dS was estimated pairwise between these strains
584 from core genome alignments using the method of Yang and Nielsen[43], as implemented in
585 Paml v4.7.
586
587 To calculate the numbers of excess mutations observed in the Asian populations, the mean
588 number of non-synonymous mutations was calculated for African and Asian populations,
589 and the difference was then multiplied by a correction factor of 1.37 to account for the loss
590 of some coding sites in the core genome alignment (1.11Mb) compared with the reference
591 genome (1.52Mb).
592
593 **Ancestry and mutation score analysis**
594 Using *H. acinonychis* as a reference, non-synonymous and synonymous mutations were
595 called against representative strains from the African and Asian populations. For this
596 analysis the ancestral populations were combined to reduce the ancestry components to
597 either African (hpAfrica) or Asian (hpAsia). For each site, the frequencies of these mutations
598 within each ancestral population were calculated to give a score between 0 and 1. These
599 scores were then combined by subtracting the hpAsia scores from the hpAfrica scores to
600 give a score between -1 and 1, where -1 = fixed in hpAsia and absent in hpAfrica, 0 = equal

601 frequencies in hpAsia and hpAfrica, 1 = absent in hpAsia and fixed in hpAfrica. Thus, these
602 scores represent the mutational load for each site in the ancestral populations. We then
603 combined these site-by-site scores with the site-by-site chromosome painting data for the
604 European populations so that each site had an estimate of ancestry component from both
605 Asia and Africa, and a mutational score representing the mutational load in the ancestral
606 populations.
607
608 We then computed linear regressions of hpAsian ancestry against mutation score for each
609 European population, and we did this for the positive (excess African) and negative (excess
610 Asian) mutation scores separately. To confirm that the regression slopes were not driven by
611 a small number of outlier genes we conducted a gene-by-gene jackknife by repeating the
612 regressions but removing all the sites from a single gene each time. From this distribution of
613 slope values we calculated the pseudovalues as pseudovalue=slope-((n-1)*(j_slope-slope)).
614 We then calculated the mean and confidence limits of these pseudovalues as
615 mean(pseudovalues) ± quantile(p=0.05/2, df=n-1) * se(pseudovalues).All data manipulation
616 and statistical analysis was performed in R 3.6.1. Packages from the 'tidyverse' collection
617 were used extensively, and ggplot2 was used for plotting.
618
619 **PCA**
620 The PCA was realized using the software PLINK v1.90 [44]on biallelic SNPS from the core
621 genome CDS of *H. pylori.* The filtered SNPs were first LD pruned using the same software to
622 get independent SNPs.
623
624 **Rate of non-adaptive non-synonymous substitutions relative to neutral divergence**
625 The rate of non-adaptive non-synonymous amino-acid substitutions relative to neutral
626 divergence was calculated based on the method of Galtier[20] and implemented in the
627 software GRAPES [20]. The software was run with folded SFS obtained from the core CDS as
628 input and no divergence data. The synonymous and non-synonymous folded SFS were
629 obtained using the PopGenome library [46] in R[45], and the number of synonymous and non-
630 synonymous sites was estimated based on the reference core genome sequence.
631
632 **Admixture graphs**
633 Admixture graphs between the different populations were obtained using the software
634 Treemix v1.12 [12]. Treemix was run with a number of migration edges between 0 to 15, with
635 10 replicates for each number of edge and hpAfrica2 was set as the outgroup. The final
636 number of migration edges was chosen as being the smallest number that allowed 99.8% of
637 the variance to be explained, which is the same criterion used by[12].
638
639 **Simulation of bacterial populations evolving under deleterious mutation pressure.**
640 We used SLiM v3 [47] to simulate the accumulation of deleterious mutations in bacterial
641 populations. Each bacterial genome was a single haploid chromosome of length 1.6 Mb,
642 with a mutation rate per site per generation of $5x10^{-7}$. This corresponds to about 1/20 of the
643 mutation rate per year estimated from *H. pylori* data [28 48]. Half of the mutations are neutral,
644 with the other half being deleterious with six different selection coefficients ($-5x10^{-3}$, $-2x10^{-}$

^{3}, -10^{-3}, $-5x10^{-4}$, $-2x10^{-4}$, -10^{-4}), each accounting for 1/12 of the mutations. There is no back mutation and mutations have a multiplicative effect on the fitness.
At the beginning of the simulation, there is no variation in the population. These parameters resulted in an intermediate mutation load for each strain. Higher mutation rates would have led to excessive load in each bacterial generation, while smaller selection coefficients would have led to individual deleterious mutations behaving as if they were neutral.

In each generation, recombination happens between strains from the same population via the transfer of one segment from a donor strain into a recipient strain, with the length of the block taken from an exponential distribution. We used three different mean values, 0, 5,000 and 50,000bp. *H. pylori* has a high rate of import of tracts with mean around 400bp [49] but simulating larger tracts is more computationally efficient than simulating many tracts.

A single population of size 10,000 evolves for 5,000 generations, by which time the population was in approximate mutation-selection equilibrium. 1,000 of the strains are moved into a second population, which retains this size for 500 generations before expanding to size 10,000. This is substantially below estimated ancestral population sizes of 2,000,000 or more for *H. pylori* [6] but sizes substantially in excess of this are difficult to simulate due to memory and computation time issues. From generation 8,000 onwards, migration from the non-bottleneck to the bottleneck populations happens at a rate of one strain every 500 generations. The simulations are completed after 15,000 total generations. Simulation output was analysed using python and R. For each population, we calculated its average fitness, its fitness variance, its dN/dS to the ancestor and within population dN/dS. Subsequent to admixture, the ancestry proportion from each population was tabulated based on mutations that had arisen during the separate evolution of the populations prior to mixture. For sites without such mutations, their origin was assumed to be the same as the closest mutation of known ancestry, provided that the mutation was within 1kb. Otherwise, its origin was recorded as unknown.
The SLiM , python and R scripts can be found at
https://github.com/EliseTourrette/scriptPubli/tree/main/ThorpeEtAl2021.

Acknowledgements:
The authors thank Sabrina Woltemate for technical assistance. This work was supported by Sequencing Grants-in-aid for Scientific Research from the Ministry of Education, Culture, Sports, Science, and Technology (MEXT) of Japan (221S0002 and 18KK0266) to YY. FFV is financed by FCT through Assistant Researcher grant CEECIND/03023/2017. KT and the sequencing of KI isolates was supported by Erik Philip-Sörensen Foundation grant G2016-08, and Swedish Society for Medical research (SSMF). All primary bioinformatics and parts of the comparative genomics were performed on resources provided by Swedish National Infrastructure for Computing (SNIC) through Uppsala Multidisciplinary Center for Advanced Computational Science (UPPMAX) under projects snic2018-8-24 and uppstore2017270.

Work by SS was supported by the German Research Foundation (DFG, project number 158 989 968–SFB 900/A1) and by the Bavarian Ministry of Science and the Arts in the framework of the Bavarian Research Network 'New Strategies Against Multi-Resistant Pathogens by Means of Digital Networking – bayresq.net. DF was supported by Shanghai Municipal Science and Technology Major Project No. 2019SHZDZX02.

Supplementary Figures:

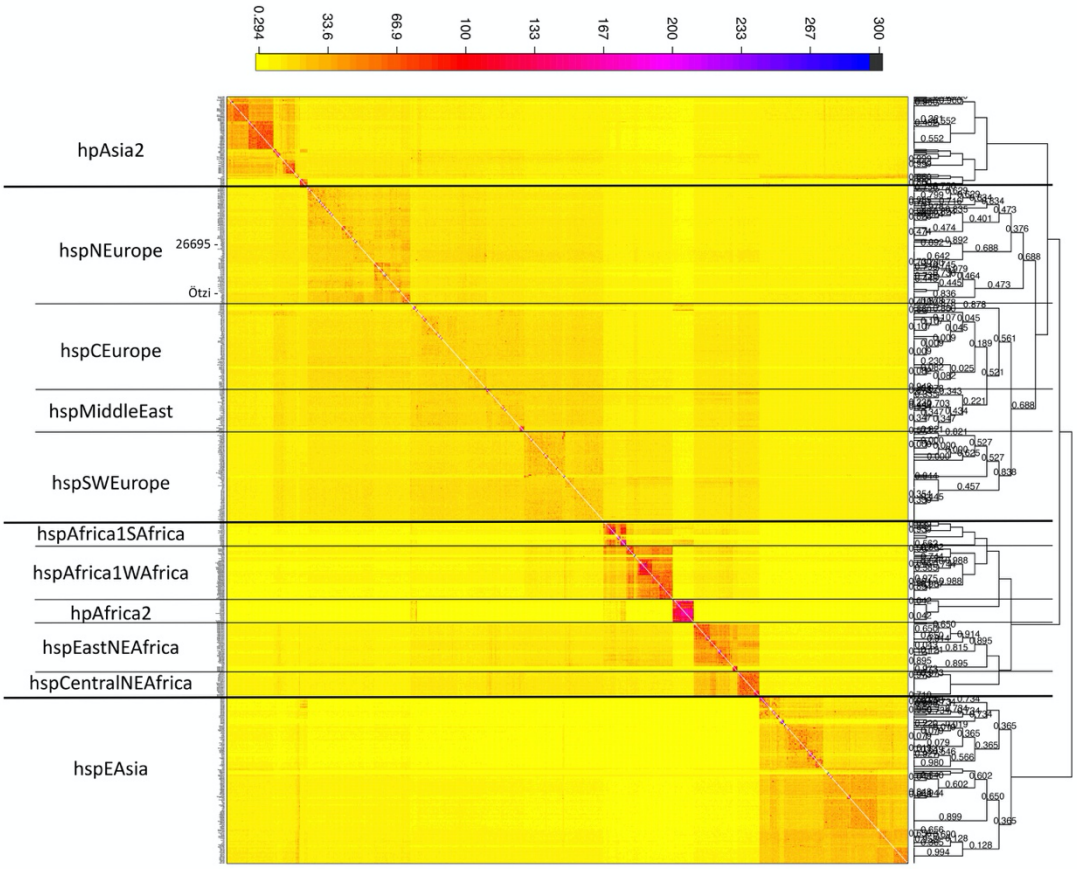

Figure S1 *heatmap showing populations inferred by fineSTRUCTURE. For each individual, the number of chunks donated by other individuals are shown according to the colour scale at the top. Note the position of Ötzi within hpsNEurope. The tree on the right shows hierarchical clustering of fineSTRUCTURE populations.*

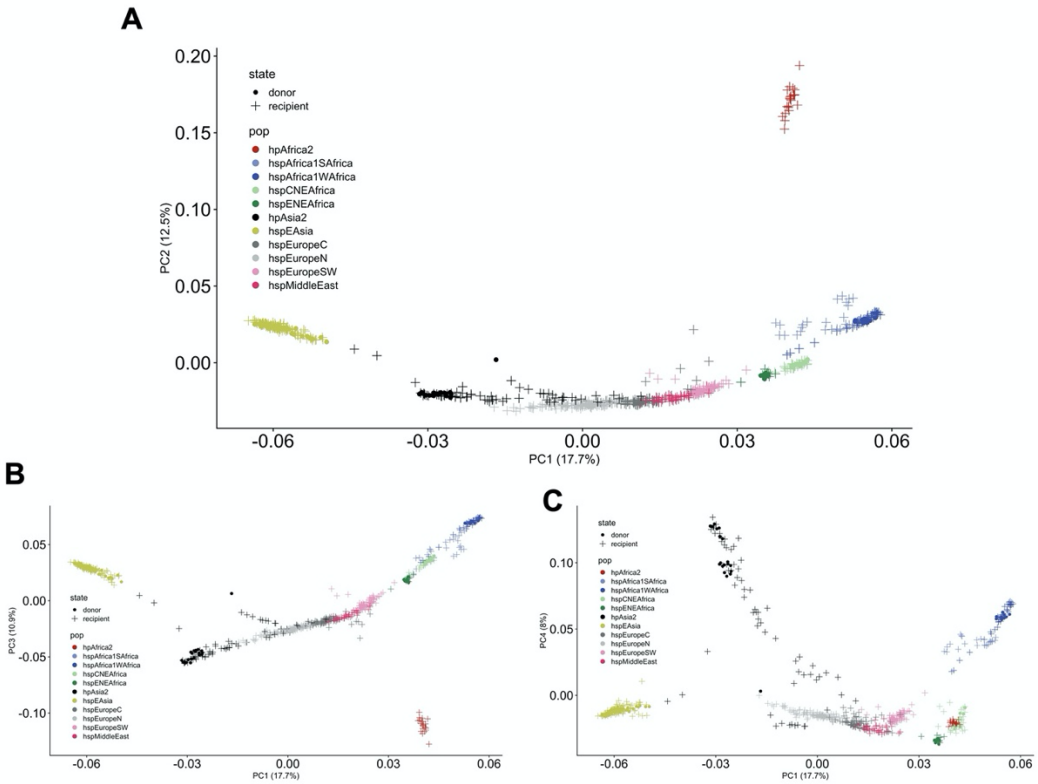

Figure S2: *First four components of a PCA showing the different African, Asian and European populations. Strains used as donors in the fineSTRUCTURE analysis are shown as circles while the recipient are shown as crosses. (A) PC2 vs PC1, (B) PC3 vs PC1 and (C) PC4 vs PC1.*

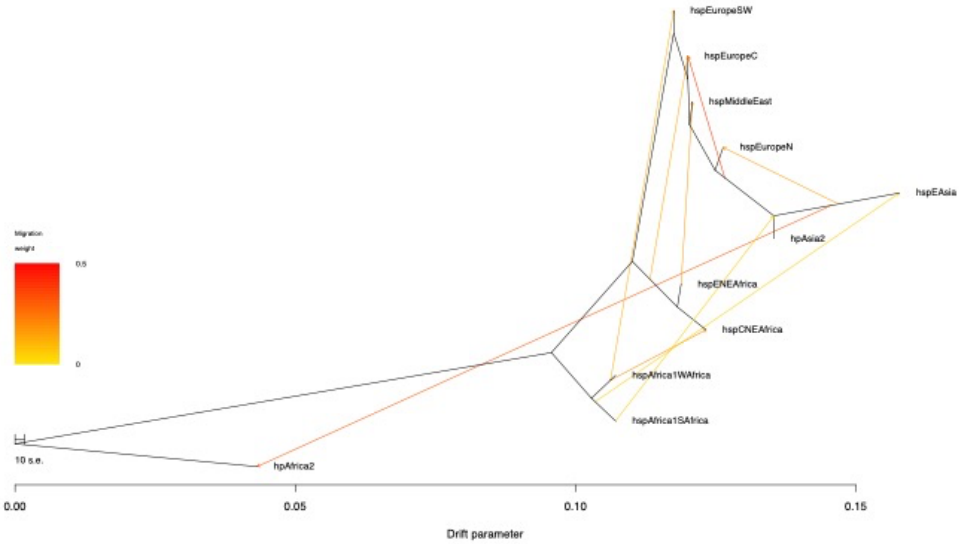

Figure S3: *Admixture graph for the different populations, with nine migration edges – the optimum number of migration edges. The population hpAfrica2 was set as the outgroup. The*

709 *arrows represent the gene flows between the different branches, their color indicating the*
710 *weight of the migration edge.*
711

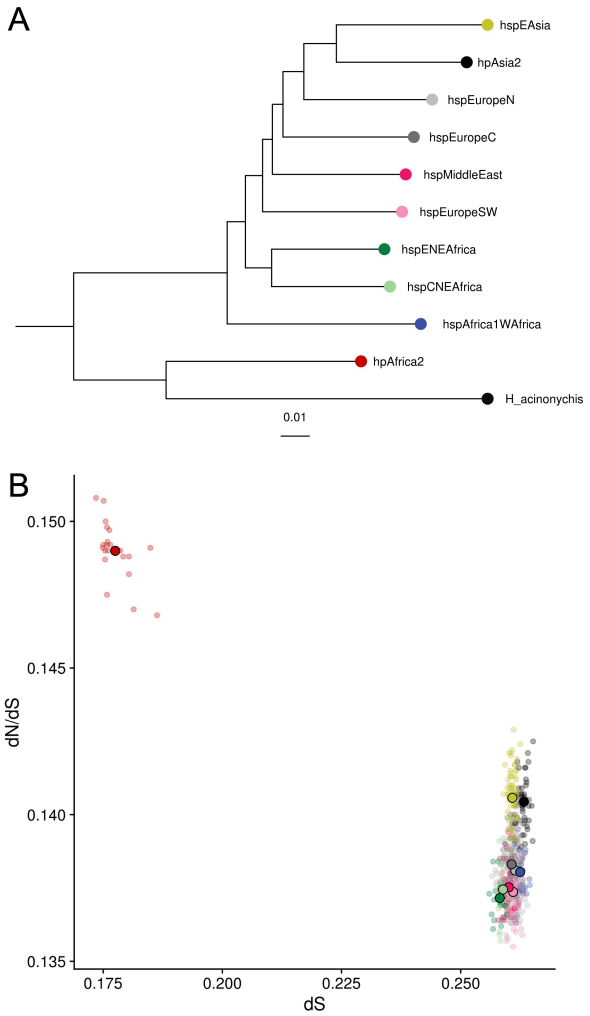

712
713 ***Figure S4*** *Relationships amongst populations. (A) Neighbor joining tree based on genetic*
714 *distances between populations. (B) dN/dS plotted against dS to H. acinonychis outroups for*
715 *all populations, including Africa2.*
716

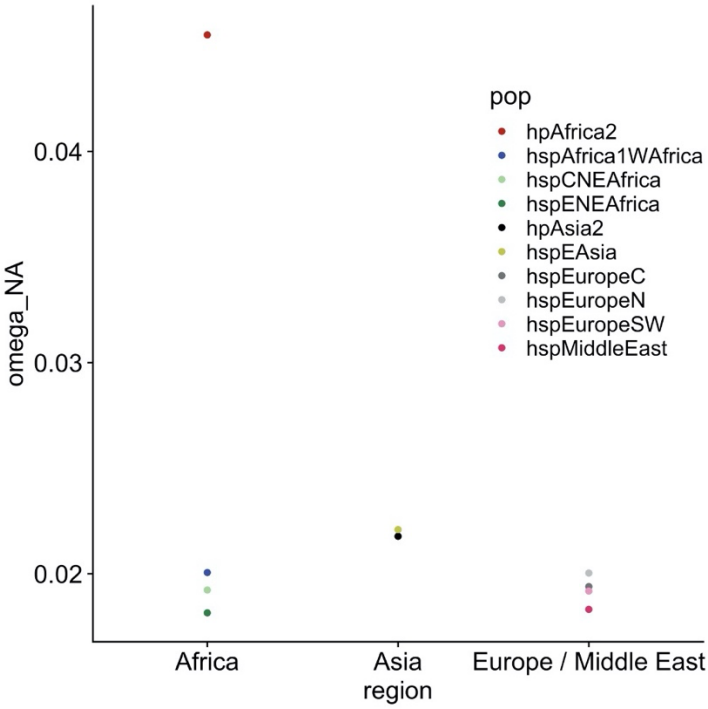

Figure S5: *Rate of non-adaptive non-synonymous amino-acid substitutions relative to neutral divergence for the different populations, separated based on the different geographical regions on the x-axis.*

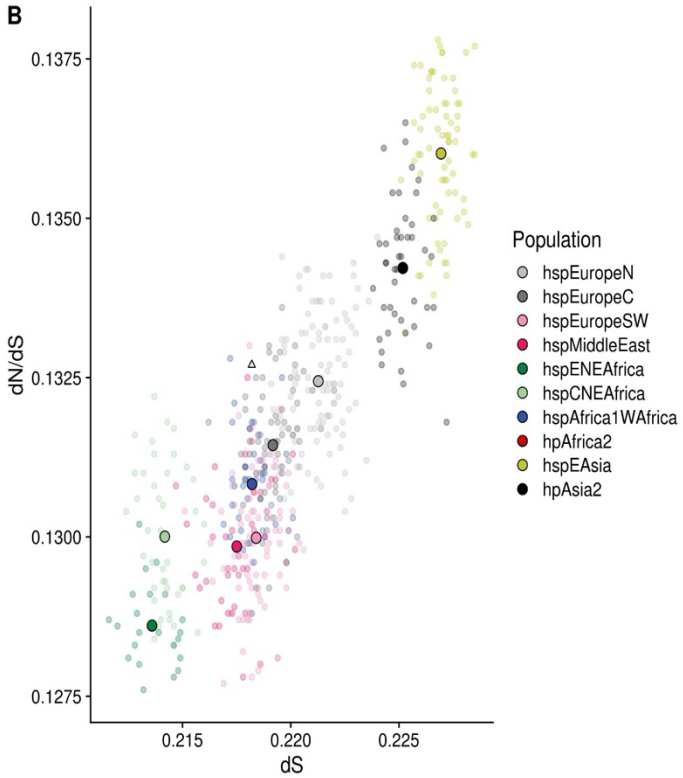

Figure S6: *Same as Figure 2B but with hpAfrica2 set as the outgroup.*

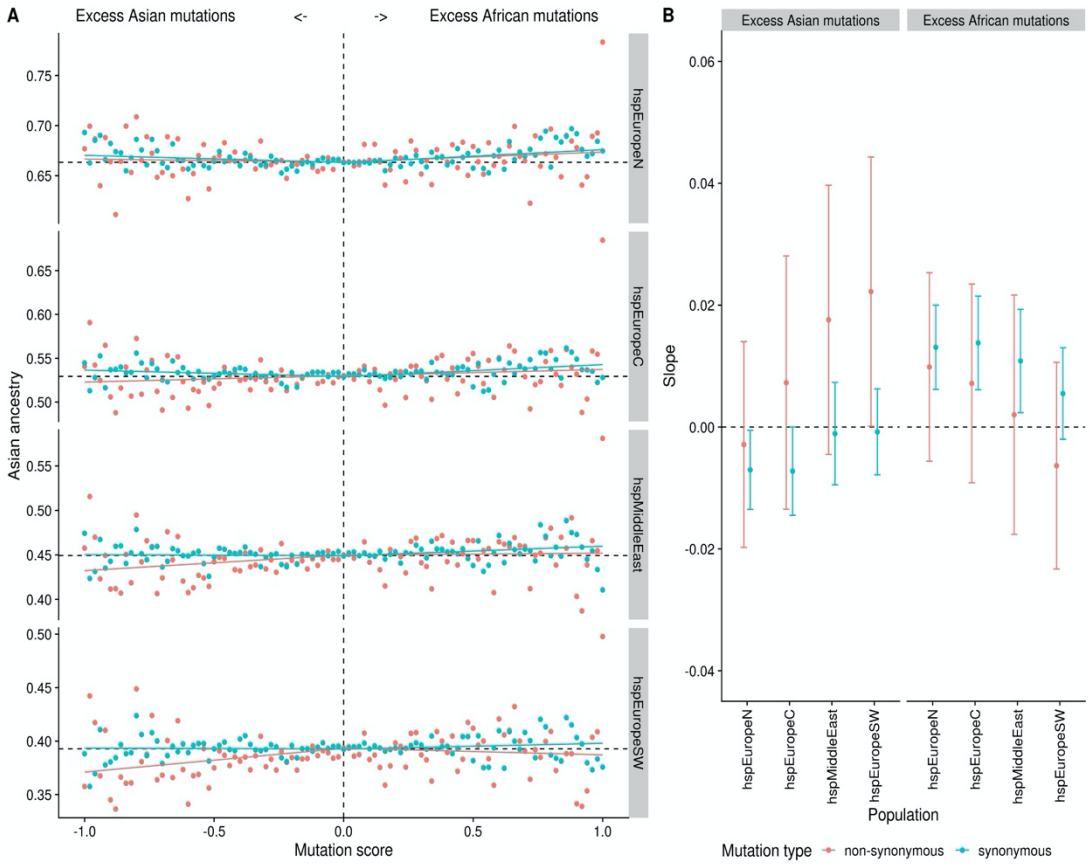

Figure S7: *Same as Figure 3 but with hpAfrica2 set as the outgroup.*

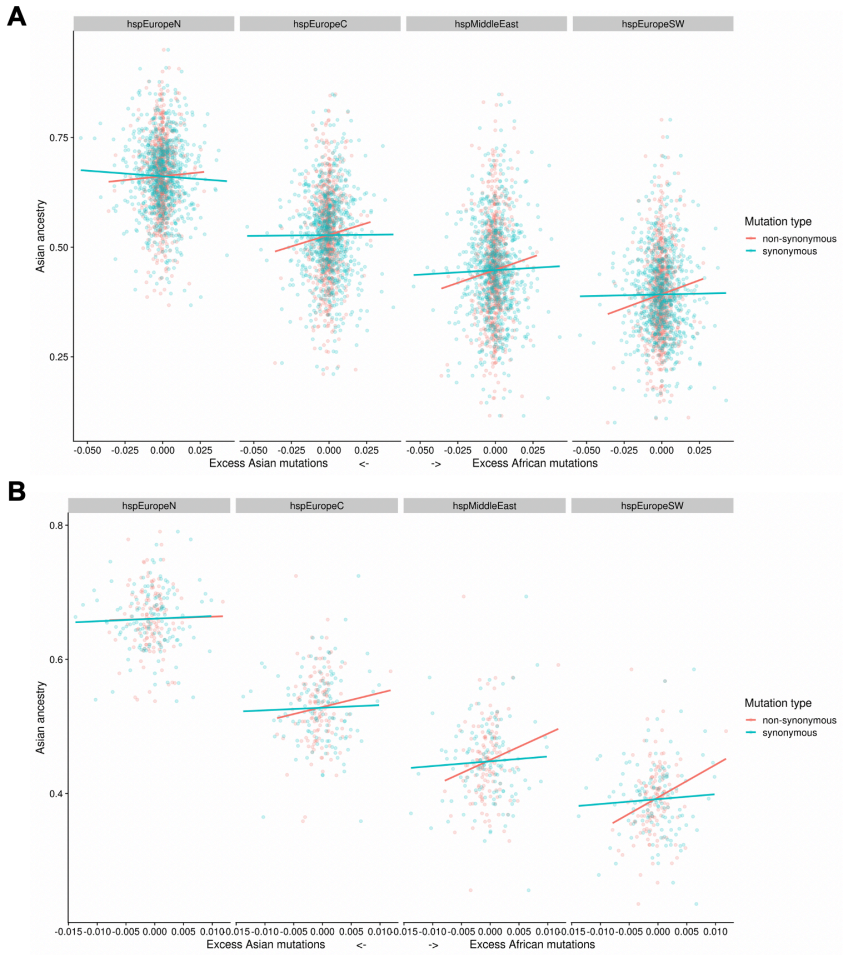

Figure S8: *Average ancestry in chromosome painting analyses plotted against mutation score (mutation frequency in African population minus mutation frequency in Asian population) (A) by genes and (B) by 10 kb bins. In both cases, only the regression in hspEuropeSW, for the non-synonymous sites, is significative.*
Regression lines are calculated separately for positive and negative mutation scores

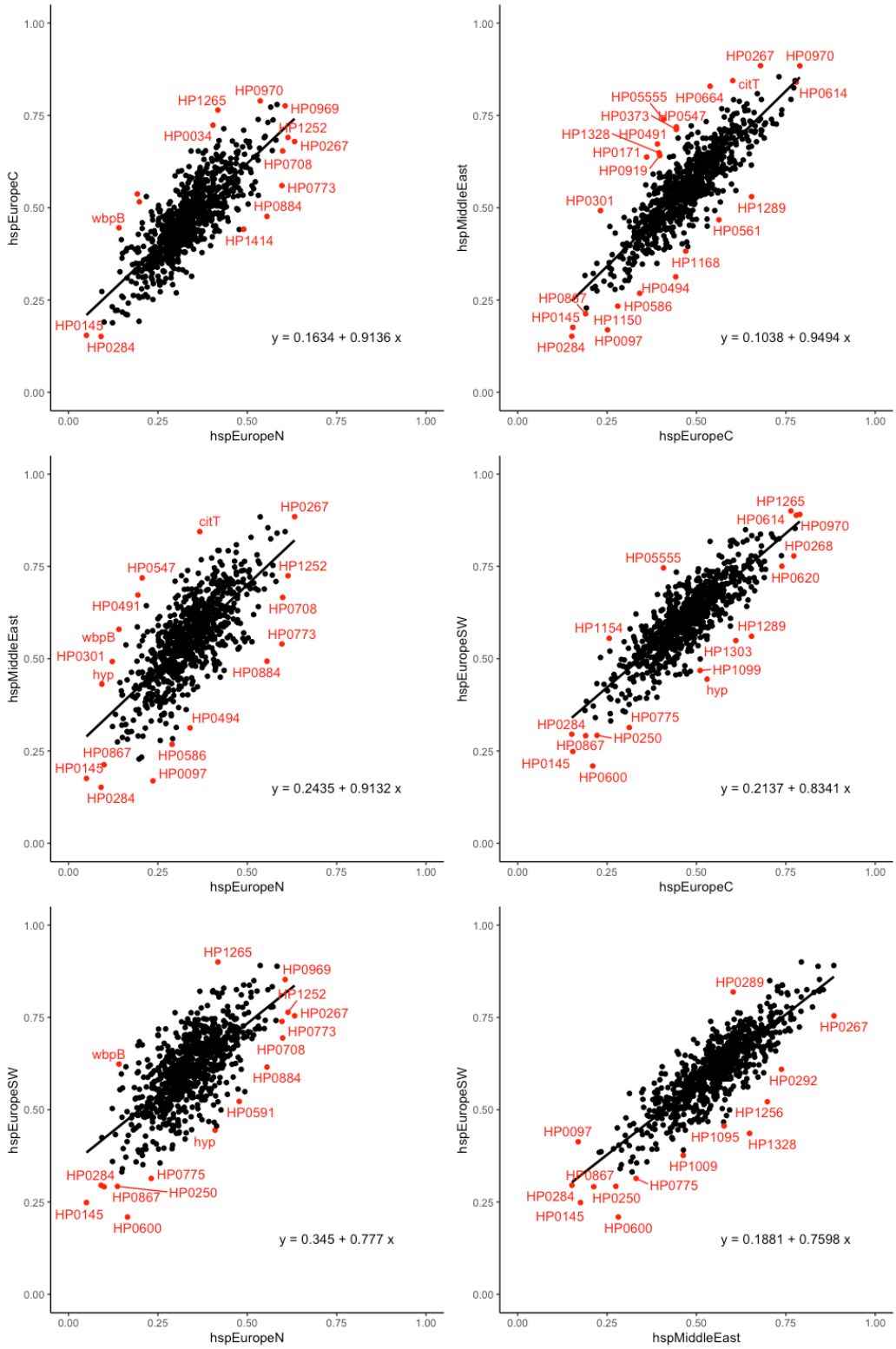

Figure S9 *Average African ancestry proportions of genes.*

Each panel shows the relationship between the proportion of ancestry assigned to Africa in the chromosome painting for each gene, for pairs of hpEurope subpopulations. Outliers from the regression slope are calculated based on robust Mahalanobis distances using the R function aq.plot(data, quan =1,alpha =0.015).

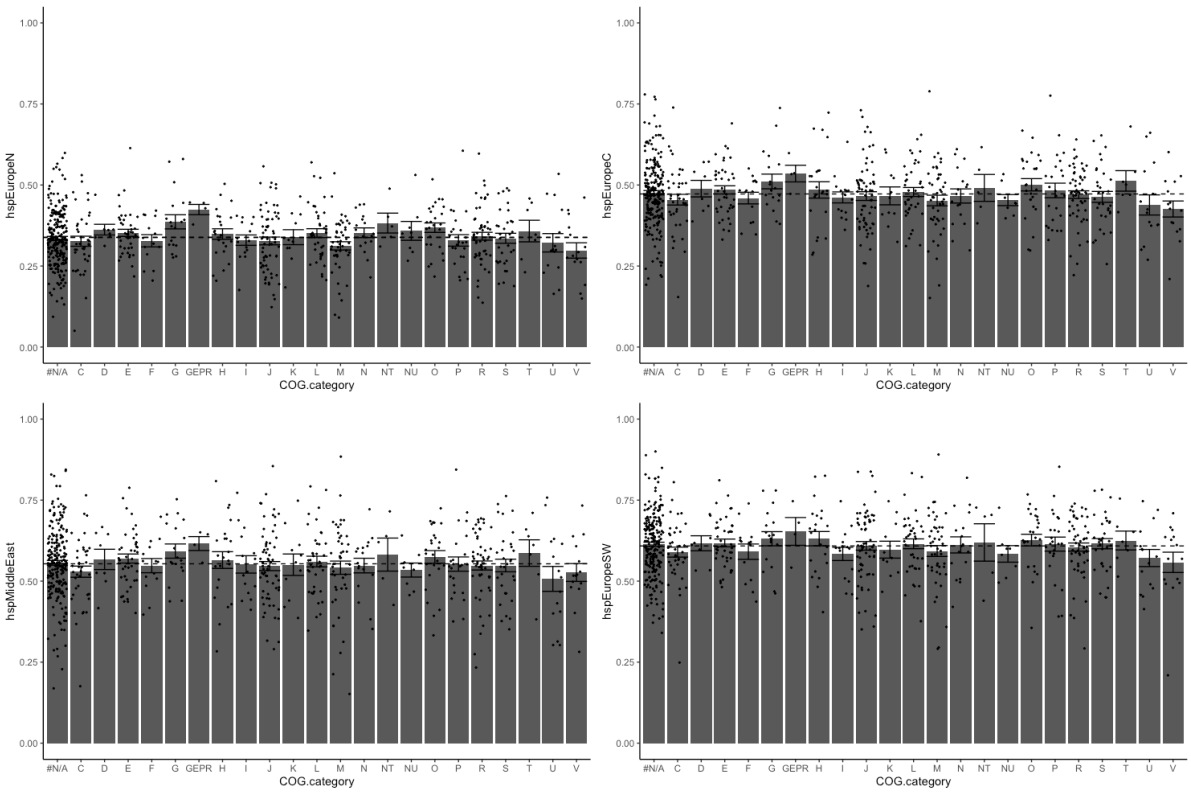

Figure S10 *Average African ancestry proportion of genes in particular COG category. Calculated separately for each hpEurope subpopulation. Whiskers show standard error of the average for each category.*

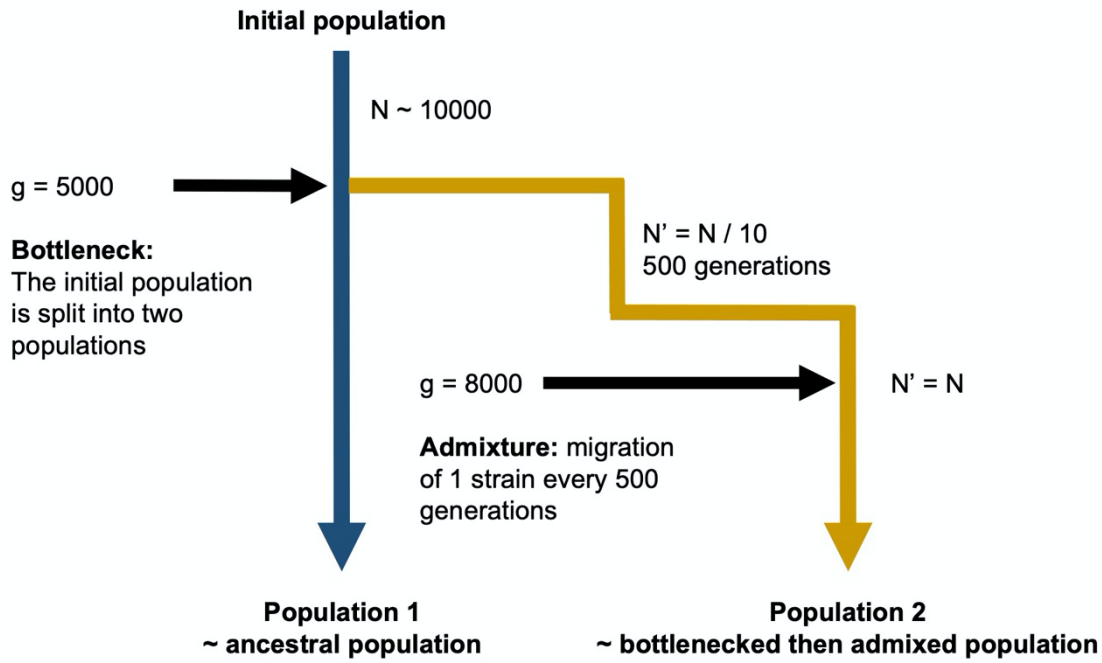

Figure S11 *The different steps of the simulation process.*
Parameters values: N = 10000; genome length = 1.6 Mbp; mutation rate = $5x10^{-7}$ per bp per generation; deleterious mutations: s = (-0.005, -0.002, -0.001, -0.0005, -0.0002, -0.0001) and they represent 50% of the mutations (the other 50% are neutral mutations). Look at different recombination levels: clonal reproduction (import size per generation = 0bp), intermediate recombination levels (import size per generation = 500bp and 5000bp on average) and nearly free recombination (import size per generation = 50000bp on average).

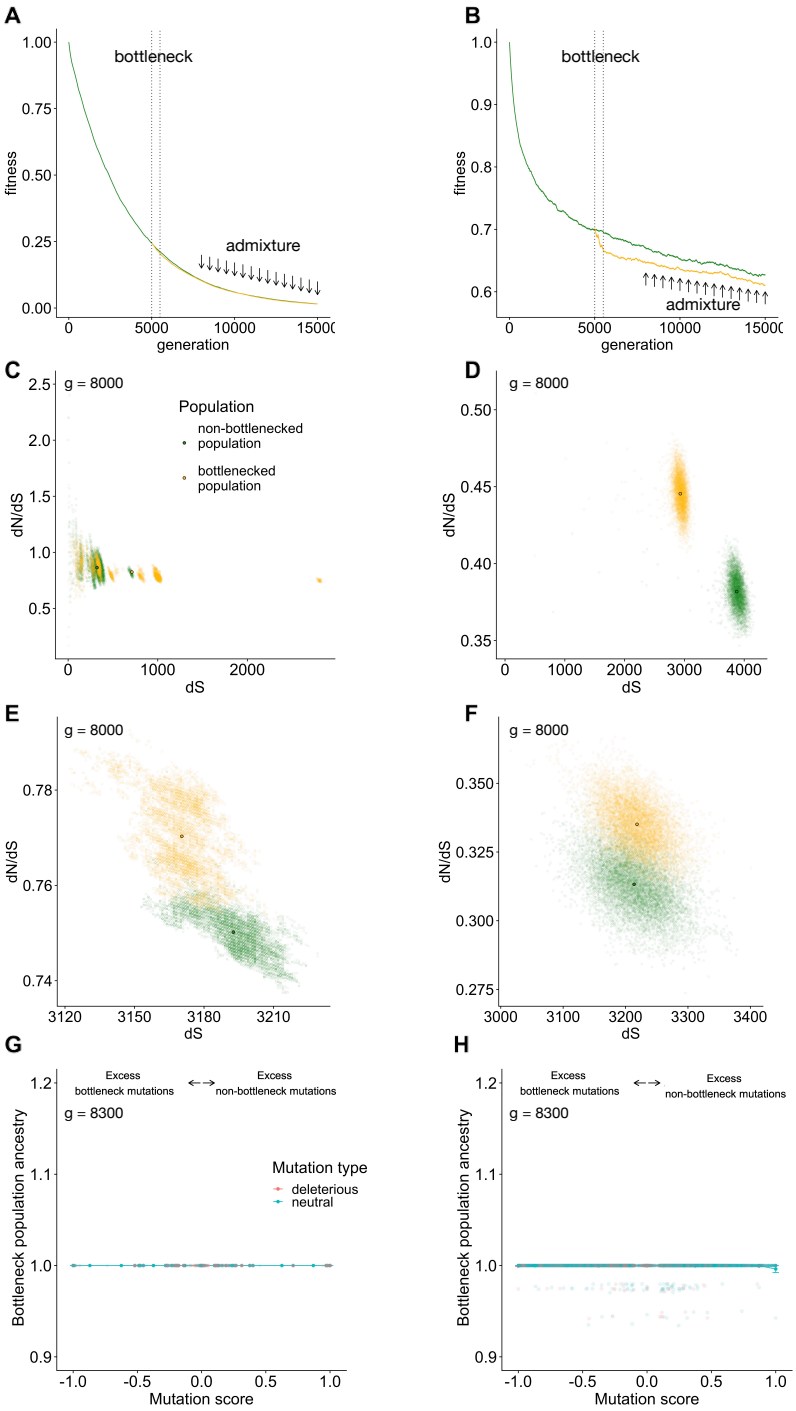

Figure S12 *The effect of different recombination rates.*
(A-B) Average fitness over the generations. (C-D) Within population dN/dS (y axis) plotted against dS (x axis). Semi opaque points show pairwise distances; solid points indicate population means. (E-F) dN/dS calculated to the ancestor plotted against dS for isolates (semi opaque points) and populations (solid points). (G-H) Average bottleneck population ancestry, after the first migration event, plotted against mutation score (frequency in the non-bottleneck population minus the frequency in the bottleneck population before the

admixture begins), under no recombination (A,C,E,G) and high recombination (B,D,F,H). The segment represents the bottleneck and the arrow signal the migration events.

References

1. Suerbaum, S. & Michetti, P. Helicobacter pylori infection. *N Engl J Med* **347**, 1175-86 (2002).
2. Schwarz, S. *et al.* Horizontal versus familial transmission of Helicobacter pylori. *PLoS Pathog* **4**, e1000180 (2008).
3. Falush, D. *et al.* Traces of human migrations in Helicobacter pylori populations. *Science* **299**, 1582-5 (2003).
4. Linz, B. *et al.* An African origin for the intimate association between humans and Helicobacter pylori. *Nature* **445**, 915-918 (2007).
5. Thorell, K. *et al.* Correction: Rapid evolution of distinct Helicobacter pylori subpopulations in the Americas. *PLoS Genet* **13**, e1006730 (2017).
6. Montano, V. *et al.* Worldwide Population Structure, Long-Term Demography, and Local Adaptation of Helicobacter pylori. *Genetics* **200**, 947-63 (2015).
7. Moodley, Y. *et al.* Age of the association between Helicobacter pylori and man. *PLoS Pathog* **8**, e1002693 (2012).
8. Maixner, F. *et al.* The 5300-year-old Helicobacter pylori genome of the Iceman. *Science* **351**, 162-165 (2016).
9. Oleastro, M., Rocha, R. & Vale, F.F. Population genetic structure of Helicobacter pylori strains from Portuguese-speaking countries. *Helicobacter* **22**(2017).
10. Hellenthal, G. *et al.* A genetic atlas of human admixture history. *Science* **343**, 747-751 (2014).
11. Patterson, N. *et al.* Ancient admixture in human history. *Genetics* **192**, 1065-93 (2012).
12. Pickrell, J.K. & Pritchard, J.K. Inference of population splits and mixtures from genome-wide allele frequency data. *PLoS Genet* **8**, e1002967 (2012).
13. Henn, B.M., Cavalli-Sforza, L.L. & Feldman, M.W. The great human expansion. *Proc Natl Acad Sci U S A* **109**, 17758-64 (2012).
14. Lynch, M., Conery, J. & Burger, R. Mutational Meltdowns in Sexual Populations. *Evolution* **49**, 1067-1080 (1995).
15. Silander, O.K., Tenaillon, O. & Chao, L. Understanding the evolutionary fate of finite populations: the dynamics of mutational effects. *PLoS Biol* **5**, e94 (2007).
16. Muller, H.J. The Relation of Recombination to Mutational Advance. *Mutat Res* **106**, 2-9 (1964).
17. Takeuchi, N., Kaneko, K. & Koonin, E.V. Horizontal gene transfer can rescue prokaryotes from Muller's ratchet: benefit of DNA from dead cells and population subdivision. *G3 (Bethesda)* **4**, 325-39 (2014).
18. Lohmueller, K.E. *et al.* Proportionally more deleterious genetic variation in European than in African populations. *Nature* **451**, 994-7 (2008).
19. Simons, Y.B. & Sella, G. The impact of recent population history on the deleterious mutation load in humans and close evolutionary relatives. *Curr Opin Genet Dev* **41**, 150-158 (2016).
20. Galtier, N. Adaptive Protein Evolution in Animals and the Effective Population Size Hypothesis. *PLoS Genet* **12**, e1005774 (2016).

21. Lafay, B., Atherton, J.C. & Sharp, P.M. Absence of translationally selected synonymous codon usage bias in Helicobacter pylori. *Microbiology (Reading)* **146 (Pt 4)**, 851-860 (2000).
22. You, Y. *et al.* Genomic differentiation within East Asian Helicobacter pylori. *Microb Genom* **8**(2022).
23. Kimura, M., Maruyama, T. & Crow, J.F. The Mutation Load in Small Populations. *Genetics* **48**, 1303-12 (1963).
24. Kim, B.Y., Huber, C.D. & Lohmueller, K.E. Deleterious variation shapes the genomic landscape of introgression. *PLoS Genet* **14**, e1007741 (2018).
25. Harris, K. & Nielsen, R. The Genetic Cost of Neanderthal Introgression. *Genetics* **203**, 881-91 (2016).
26. Schumer, M. *et al.* Natural selection interacts with recombination to shape the evolution of hybrid genomes. *Science* **360**, 656-660 (2018).
27. Liu, S. *et al.* Demographic History and Natural Selection Shape Patterns of Deleterious Mutation Load and Barriers to Introgression across Populus Genome. *Mol Biol Evol* **39**(2022).
28. Didelot, X. *et al.* Genomic evolution and transmission of Helicobacter pylori in two South African families. *Proc Natl Acad Sci U S A* **110**, 13880-5 (2013).
29. Suerbaum, S. *et al.* Free recombination within Helicobacter pylori. *Proc Natl Acad Sci U S A* **95**, 12619-24 (1998).
30. Chao, Y., Cui, Y., Didelot, X., Yang, X. & Falush, D. Why panmictic bacteria are rare. *Bioarxiv* (2018).
31. Morelli, G. *et al.* Microevolution of Helicobacter pylori during prolonged infection of single hosts and within families. *PLoS Genet* **6**, e1001036 (2010).
32. Duncan, S.S. *et al.* Comparative genomic analysis of East Asian and non-Asian Helicobacter pylori strains identifies rapidly evolving genes. *PLoS One* **8**, e55120 (2013).
33. Wright, S. The shifting balance theory and macroevolution. *Annu Rev Genet* **16**, 1-19 (1982).
34. Bankevich, A. *et al.* SPAdes: a new genome assembly algorithm and its applications to single-cell sequencing. *J Comput Biol* **19**, 455-77 (2012).
35. Bolger, A.M., Lohse, M. & Usadel, B. Trimmomatic: a flexible trimmer for Illumina sequence data. *Bioinformatics* **30**, 2114-20 (2014).
36. Gurevich, A., Saveliev, V., Vyahhi, N. & Tesler, G. QUAST: quality assessment tool for genome assemblies. *Bioinformatics* **29**, 1072-5 (2013).
37. Zerbino, D.R. & Birney, E. Velvet: algorithms for de novo short read assembly using de Bruijn graphs. *Genome Res* **18**, 821-9 (2008).
38. Seemann, T. Prokka: rapid prokaryotic genome annotation. *Bioinformatics* **30**, 2068-9 (2014).
39. Resende, T., Correia, D.M., Rocha, M. & Rocha, I. Re-annotation of the genome sequence of Helicobacter pylori 26695. *J Integr Bioinform* **10**, 233 (2013).
40. Ewels, P., Magnusson, M., Lundin, S. & Kaller, M. MultiQC: summarize analysis results for multiple tools and samples in a single report. *Bioinformatics* **32**, 3047-8 (2016).
41. Lawson, D.J., Hellenthal, G., Myers, S. & Falush, D. Inference of population structure using dense haplotype data. *PLoS Genet* **8**, e1002453 (2012).
42. Yahara, K. *et al.* Chromosome painting in silico in a bacterial species reveals fine population structure. *Mol Biol Evol* **30**, 1454-64 (2013).
43. Yang, Z. & Nielsen, R. Estimating synonymous and nonsynonymous substitution rates under realistic evolutionary models. *Mol Biol Evol* **17**, 32-43 (2000).

44. Chang, C.C. *et al.* Second-generation PLINK: rising to the challenge of larger and richer datasets. *Gigascience* **4**, 7 (2015).
45. Team, R.C. R: A language and environment for statistical computing. (2021).
46. Pfeifer, B., Wittelsburger, U., Ramos-Onsins, S.E. & Lercher, M.J. PopGenome: an efficient Swiss army knife for population genomic analyses in R. *Mol Biol Evol* **31**, 1929-36 (2014).
47. Haller, B.C. & Messer, P.W. Evolutionary Modeling in SLiM 3 for Beginners. *Mol Biol Evol* **36**, 1101-1109 (2019).
48. Falush, D. *et al.* Recombination and mutation during long-term gastric colonization by Helicobacter pylori: estimates of clock rates, recombination size, and minimal age. *Proc Natl Acad Sci U S A* **98**, 15056-61 (2001).
49. Kennemann, L. *et al.* Helicobacter pylori genome evolution during human infection. *Proc Natl Acad Sci U S A* **108**, 5033-8 (2011).